P197

Evaluation of the Baseline NEXRAD Icing Hazard Product*

Michael F. Donovan, Earle R. Williams, David J. Smalley,
Robert G. Hallowell, and Betty J. Bennett,
Massachusetts Institute of Technology, Lincoln Laboratory

1. INTRODUCTION

The Icing Hazard Levels (IHL) algorithm has been operational within the U.S. Next Generation Weather Radar (NEXRAD) system since early 2014. IHL incorporates detection products generated from other NEXRAD algorithms; such as, the Hydrometeor Classification Algorithm (HCA), the Melting Layer Detection Algorithm (MLDA), and gridded one-hour Numerical Weather Prediction (NWP) Rapid Refresh (RAP) forecast fields, to produce a top and bottom icing hazard altitude product that defines the bounds of an icing layer derived at each radar range-azimuth bin. With sponsorship from the Federal Aviation Administration (FAA), MIT Lincoln Laboratory (LL) developed this algorithm to provide high resolution spatial and temporal icing products that depict the icing hazard within the radar space and can be used as an adjunct to other icing diagnosis and forecast products such as the National Weather Service's (NWS) Current and Forecast Icing Potential (CIP/FIP) products and observed pilot reports (PIREPs) of icing. Details of the IHL algorithm are described in Hallowell et al. (2013). Prior to operational deployment, the icing hazard product was verified against a small set of PIREPs. The focus of this report is to assess the baseline IHL algorithm performance through a comprehensive study where PIREPs collected over a two-month period in close proximity to 23 NEXRAD sites were used for validation. These results drive future focus from which subsequent modifications will be implemented and performance reevaluated.

* This work was sponsored by the Federal Aviation Administration under Air Force Contract FA8721-05-C-0002. Opinion, interpretations, conclusions, and recommendations are those of the authors and are not necessarily endorsed by the U.S. Government.

An overview of the IHL algorithm components is provided in Section 2. Section 3 details the verification study and the methodology used to spatially and temporally match IHL detections to a pilot reported icing location. The results obtained in this study underscore the need to evaluate and extract dual polarimetric (herein referred to as dual pol) icing signatures associated with non-Graupel classes generated by the NEXRAD HCA. Similar findings were discovered in an icing field campaign near the Buffalo, New York NEXRAD (KBUF) where in situ icing measurements were compared to the hydrometeor classification product. Case examples from these comparisons are provided in Section 4.

2. ALGORITHM

The baseline IHL algorithm ingests multiple icing-related data products available within the NEXRAD Open Radar Product Generator (ORPG) system (Ganger et al. 2002; Smalley and Bennett 2002). Figure 1 illustrates the interdependencies among the NEXRAD algorithms and the data product flow into the IHL algorithm. The algorithm components are color-coded in green, gold, and gray to indicate whether new software and data products were created, modified by MIT LL, or left undisturbed, respectively. An overview of each component algorithm follows.

The NEXRAD ORPG system receives hourly updates of the NWP RAP 13 km one-hour model forecast. Model fields include a two-dimensional grid of surface pressure and three-dimensional vertical profiles of geopotential height, temperature, relative humidity, and u- and v-wind components. The geopotential height and temperature profile data are used by the NEXRAD Melting Layer Detection Algorithm (MLDA)

(Giangrande et al. 2008) to estimate the height of the melting layer (ML) when the algorithm fails to detect a ML from radar data alone because there is insufficient evidence of a 'bright band' detection within the dual pol products. The original MLDA, however, only applies a single vertical profile from the NWP grid point closest to the radar location to the entire radar scanning domain. The absence of model information beyond the radar location often causes inaccuracies in the ML height during transitional weather events that propagate over the radar domain. To address this shortcoming, MIT LL modified the model ingest software to create derived gridded products over the entire domain such as the number of instances that the temperature profile crosses 0° C, the altitudes of each crossing, and the temperature magnitudes of each warm and cold layer beneath the highest altitude crossing found. The expanded use of these products within the MLDA allows for more accurate estimates of the ML heights when gaps occur in the radar diagnosed ML and when the radar estimate is inadequate.

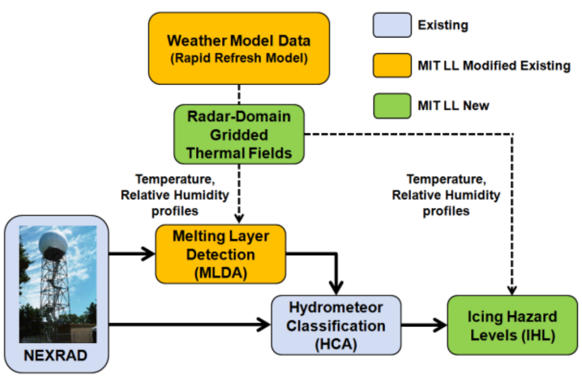

Figure 1. Illustration shows the NEXRAD component algorithm and data products flowing into the baseline NEXRAD IHL algorithm. Components are color-coded in green, gold, and gray to indicate whether new software or data products were created, modified, or left undisturbed, respectively.

The NEXRAD Hydrometeor Classification Algorithm (HCA) applies fuzzy logic and weighting schemes to the dual pol products in order to classify the radar returns into one of twelve frozen, liquid, or non-meteorological categories at each range-azimuth bin of the radar beam (Park et al. 2009). The ML information generated by the MLDA plays an important role within the HCA by allowing or restricting categorizations of the radar bin based on its location relative to the estimated ML position. While the HCA does not explicitly categorize hydrometeors for icing, it does classify graupel particles. Graupel forms from the instantaneous riming of ice crystals or snow aggregates as they encounter supercooled liquid water (SLW) upon their descent. It's usually a transitional category between frozen and liquid precipitation and is normally located within and just above the ML. MIT LL did not make any changes to this algorithm.

Figure 2 shows Plan Position Indicator (PPI) image of the HCA product from the Vance, Oklahoma NEXRAD (KVNX) on April 27, 2011 at 08:21 UTC for the 1.5° elevation angle (left) and the corresponding HCA cross section over all elevation angles within the radar volume and along the dashed azimuth line indicated (right). The black horizontal contours stacked vertically represent the NWP RAP 13 km model temperature with the 0° C contour shown in red. The Graupel class, shown as pink, resides near the ML and adjacent to the Wet Snow classifications (dark blue). The location of the HCA Graupel detections found within the radar volume forms the basis of the IHL detection algorithm. Since the size of the radar beam angle is known, the top and bottom altitudes of any radar bin are easily calculated. The IHL algorithm processes the entire radar volume such that the lowest (highest) beam angle where Graupel is found determines the radar-based altitude of the icing bottom (top) for each range-azimuth bin.

However, comparisons of PIREPs and HCA classifications often indicate that icing was encountered at altitudes above the region where Graupel was classified. The explanation for this is that the riming process that converts ice crystals or snow to graupel requires some vertical extent. Further, both the density of the ice crystals and snow along with the supply of SLW must be sufficient to create graupel in a quantity that the HCA recognizes. To account for the vertical transition zone, the NWP RAP model temperature

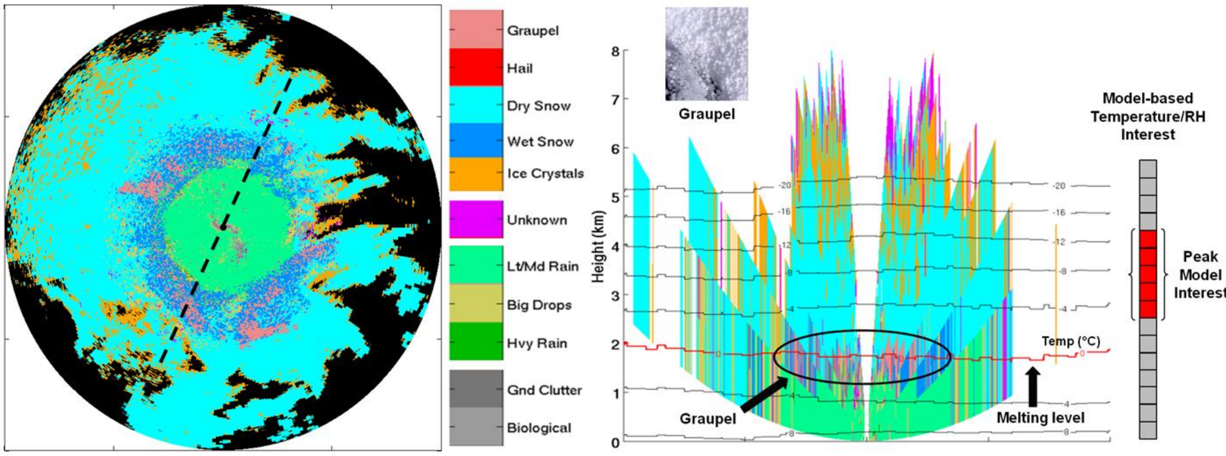

Figure 2. PPI image of the 1.5° elevation angle HCA product (left) for the Vance, Oklahoma NEXRAD (KVNX) on April 27, 2011 at 08:21 UTC and the corresponding volume cross section along the dashed line (right). The horizontal contours on the cross section image are the one-hour temperature forecast from the RAP 13 km model. The thin vertical rectangle on the far right indicates the altitude layer of the highest icing probability (shown in red) based on the model temperature and relative humidity interest product.

and relative humidity vertical profile data are converted to model interest fields by utilizing techniques in the CIP algorithm (Bernstein et al. 2005) developed at the National Center for Atmospheric Research (NCAR). The product of these interest fields is then computed to create a total model icing interest (MII) field to identify regions that may be conducive to icing based on temperature and relative humidity alone. The MII is based on a scale ranging from 0 to 1, where 1 indicates the highest probability for icing. The MII is computed over the entire radar domain but only applied to azimuth-range bin columns that contain Graupel.

In regions above the Graupel class, where HCA has classified the radar bin to some other 'cold' hydrometeor class (such as Ice Crystal or Dry Snow), the IHL algorithm searches the MII profile from the top down until the interest first exceeds a threshold value of 0.8. If the threshold level is found, the Graupel-based icing top altitude is extended vertically to the altitude where the threshold was first exceeded. Figure 3 contains a cross section of the MII product for the same example case shown in Figure 2. Note that the peak model interest region (color-coded as orange and burnt red) resides above the Graupel area (pink) shown in Figure 2 (right panel) in locations classified by HCA as Dry Snow (turquoise) and signifying where the extension of the IHL Graupel-based detections will occur.

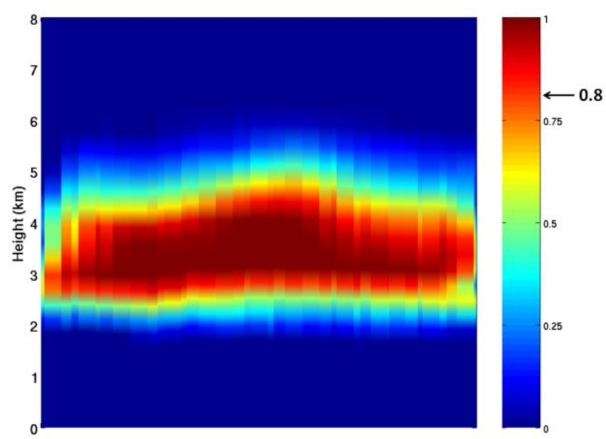

Figure 3. Cross section of the model icing interest product for the KVNX example shown in Figure 2. Peak model interest and highest probability of icing is depicted in the orange and burnt red regions.

The NEXRAD IHL produces a top and bottom altitude product once per radar volume scan time. Figure 4 shows the PPI display of the IHL top (left)

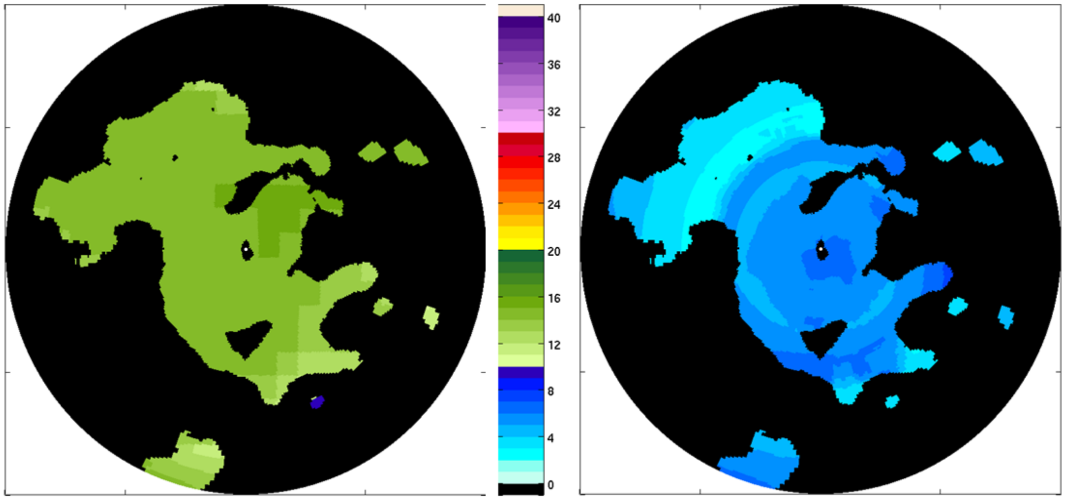

Figure 4. PPI display of the IHL top (left) and bottom (right) altitude products in kilo-feet units for the KVNX radar volume example shown in Figure 2.

and bottom (right) products that bound the icing hazard layer in kilo-feet (kft) units for the same KVNX radar example shown in Figure 2. Products are portrayed on a polar grid with a 1° by 1 km resolution out to a range of 300 km (maximum range of dual pol data). Additional IHL product components for severity and confidence will accompany the altitude aspect of the product as future techniques that address the icing hazard in non-Graupel classified regions mature.

3. IHL EVALUATION STUDY

Icing PIREPs logged by general aviation and commercial aircraft were used to validate and assess the IHL algorithm performance from several NEXRADs over different geographical regions. Pilots are encouraged but not mandated to issue a report when icing or turbulence is encountered. These reports are helpful in alerting pilots that follow in the path of the reporting aircraft and contain valuable information such as the time and location, icing type and severity, and the flight level(s) where icing was experienced but they do not capture the full extent of the icing hazard. Figure 5 shows an example distribution of icing PIREPs collected over an 80-minute period ending at 22:00 UTC on November 22, 2013 over the CONUS. These reports are readily available in real time from the NWS Aviation Weather Center (AWC) Aviation Digital Data Service (ADDS) website, www.aviationweather.gov/icing.

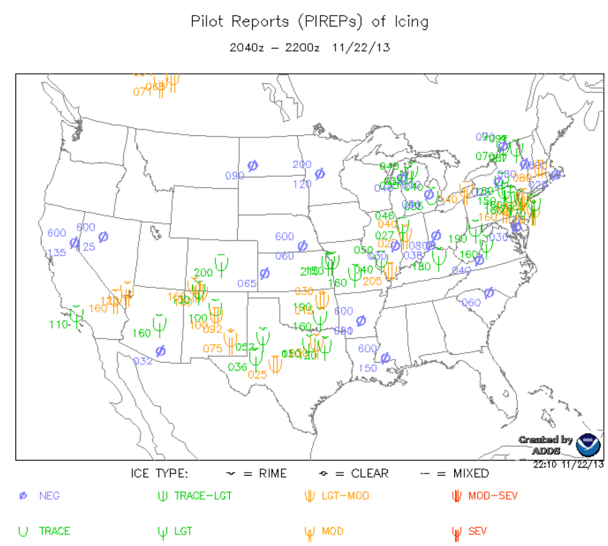

Figure 5. Distribution of icing pilot reports observed between 20:40-22:00 UTC on November 22, 2013 over the CONUS. Reports are color-coded in blue to represent no-icing observed or green, yellow, and red to indicate increasing levels of icing severity.

MIT LL operates a configurable ORPG clone test network where as many as 50 NEXRAD sites run continuously to allow algorithm product evaluation in real time and automatic product archiving for post-analysis. Prior to determining which sites would be selected for the IHL evaluation, a frequency map of PIREP reporting locations was constructed. Figure 6 shows the distribution of NEXRAD sites color-coded according to the percentage of PIREPs located within 300 km from each radar site for the three-year period 2010-2012. The highest incident reported regions occurred in the Pacific Northwest, Great Lakes, and Northeastern states. The two, red-outlined areas in Figure 6 encompass the 23 NEXRAD sites that were selected for the IHL evaluation study. The study was performed over a two-month period between February-March 2013. Two NEXRAD sites, showing the highest PIREP frequency (North Webster, IN and Detroit, MI), were not included because they were not converted to dual polarization prior to the evaluation period.

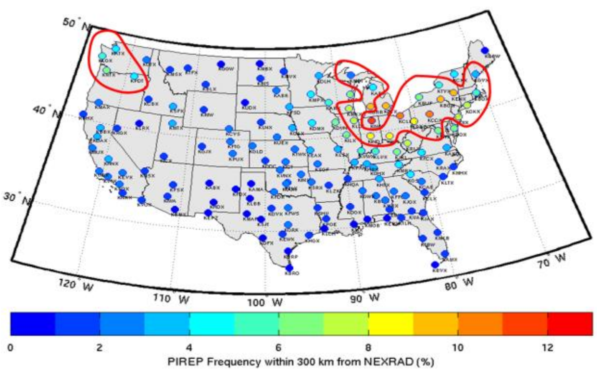

Figure 6. Map of PIREP location frequency color-coded according to the number of reports within 300 km from each NEXRAD site for all reports received from the three-year period 2010-2012. The red enclosures encompass the 23 sites where IHL-PIREP comparisons were made between February-March 2013.

3.1 PIREP Uncertainties

PIREPs provide a broad area of coverage and valuable information but the process by which icing information is recorded and disseminated can result in delayed reporting. Reporting is predominately a manual process where the pilot looks for visual cues of ice accretion on the airframe and reports the intensity of the icing encountered in a numeric severity scale. A single latitude-longitude position and report time is recorded but given that pilots may delay the issuance of the report until they have safely cleared the hazard, and that the accretion of ice takes place over some unspecified time and distance, spatial and time offsets between a pilot's reported and experienced position can occur (Schwartz, 1996). Figure 7 illustrates an example of the magnitude of these offsets that can occur.

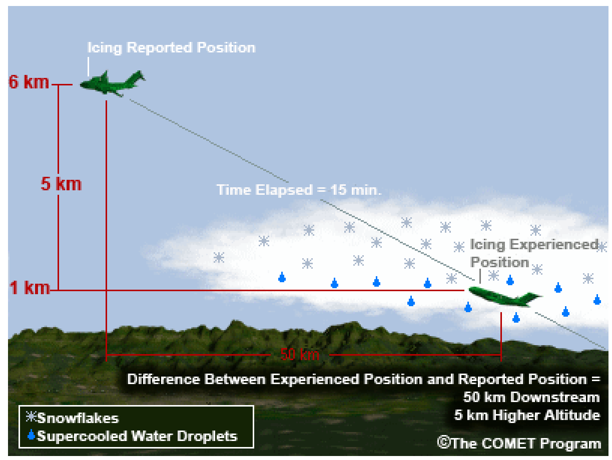

Figure 7. Illustration showing the temporal and spatial differences that can occur between the icing experienced position and the icing reported position. The source of this material is the COMET® Website at http://meted.ucar.edu/ of the University Corporation for Atmospheric Research (UCAR), sponsored in part through cooperative agreement(s) with the National Oceanic and Atmospheric Administration (NOAA), U.S. Department of Commerce (DOC). ©1997-2015 UCAR. All Rights Reserved.

To account for the PIREP spatial uncertainties in the verification study coupled with knowing that icing can exist in thin layers over long distances in stratiform winter weather systems, a cylinder centered at each PIREP location is constructed to encompass the icing airspace associated with each report. A three-dimensional illustration of the cylinder geometry is shown in Figure 8. For icing PIREPs, the cylinder is bounded by a 50 km radius and 1000 ft vertically (both above and below) from the icing encountered flight level(s). For null PIREPs (reports indicating the pilot did not observe icing), the cylinder is bounded by a 10 km radius and 500 ft vertically (again above and below). All radar bin heights, at each beam elevation angle in the volume, are first converted to mean sea level (MSL) to align with the PIREP altitude reporting standard and then checked to determine whether any bin intersects the PIREP cylinder space. For all PIREP-radar bin intersections, an outline of the cylinder geometry is extended on the polar grid surface to create a footprint from which an overlap with IHL detections can be compared. Cylinder footprint examples are shown at the bottom of Figure 8.

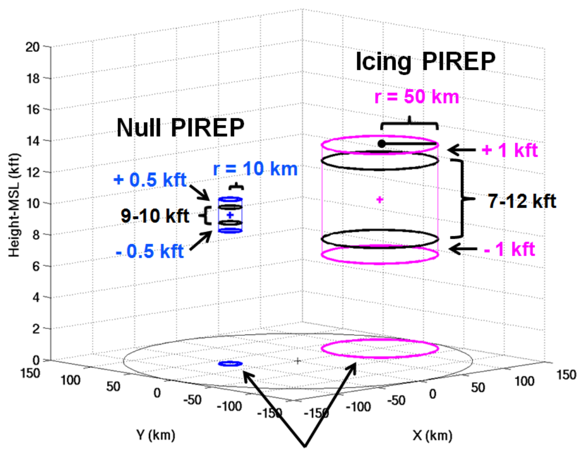

Figure 8. Three-dimensional cylinder geometries used to define the icing airspace or lack thereof associated with icing (magenta) and null (blue) PIREPs, respectively. Example PIREP flight levels are shown in black. The cylinder areas and boundary outlines depicted as footprints onto the surface plane were used in validating the IHL detections.

To account for temporal uncertainties, each PIREP-IHL comparison was considered a 'match' if IHL detections resided within the cylinder footprint for any radar volume scan that occurred within +/- 15 minutes to the PIREP report time. Depending on which volume coverage pattern (VCP) the radar was operating in, clear air or precipitation mode, there could be as many as 3-6 scans tested, respectively.

3.2 Scoring Methodology

The IHL algorithm was evaluated and scored according to the categories shown in Figure 9. The top row shows a three-dimensional view of the IHL product color-coded in cyan and PIREP cylinders in magenta. The bottom row contains the IHL product and cylinder footprint on the surface plane. For icing PIREPs, any IHL detection residing within the cylinder footprint is scored as a 'Hit' or 'Miss' if any portion of the icing top to bottom altitude layer overlaps or does not overlap the cylinder space, respectively. For null PIREPs, detections residing within the footprint with overlapping altitudes are scored as 'False Alarm' and reports where no detection overlaps the null cylinder in altitude are scored as 'Correct No Detect' (not shown in Figure 9).

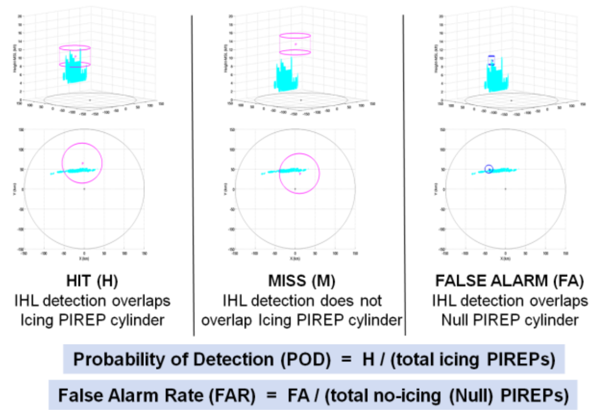

Figure 9. Illustration of three scoring categories recorded for each PIREP-IHL comparison. IHL detections are shown in cyan and PIREP cylinders are shown in magenta. The top row shows the three-dimensional view to determine overlap in altitude and the bottom row shows the projection of the cylinder onto the surface plane.

The verification statistics for the Probability of Detection (POD) and False Alarm Rate (FAR) were calculated for each NEXRAD site according to the formulas defined below.

$$POD = \frac{\text{number of HITs}}{\text{number of icing PIREPs}}$$

$$FAR = \frac{\text{number of FALSE ALARMs}}{\text{number of null PIREPs}}$$

The number of icing and null PIREPs used in these computations does not reflect a total PIREP count collected over the two-month study but rather those reports when any radar beam in the volume intersected the cylinder space. This subset number of icing PIREPs is limited further to represent cases when IHL detections were found within the cylinder footprint. Given that the baseline IHL version can only issue detections in the presence of HCA-generated Graupel classifications augmented by MII, performance should only be measured on that subset of cases. IHL detections issued outside the cylinder footprint were not evaluated due to the lack of PIREP information to verify that icing was present or absent.

It is important to note that the probabilities for POD and FAR are PIREP based and the absolute skill of the IHL algorithm to detect icing cannot be obtained. Since pilots are not required to report icing and are less likely to report no-icing conditions, the lack of PIREP information is not an indication icing is not present. In fact, during recent, major northeast U.S. snowstorms that typically involve icing hazards, there has been PIREP silence since commercial airlines have grounded their entire regional fleets. This results in an imprecise distribution of reported icing and no-icing conditions thus preventing a true estimation of the FAR and limiting the interpretation of POD (Brown et al. 1997). Nonetheless, these statistics are useful to establish the performance results of the baseline IHL algorithm for comparison with subsequent, more advanced algorithm versions using the same PIREP dataset.

Over the two-month period, a total of 7761 icing and 899 null PIREPs were included in the study. Among the icing PIREPs, 1120 reports (14%) contained Graupel within the cylinder footprint (i.e. – IHL registered a detection). The number of null PIREPs used to compute FAR for which there was a radar beam-cylinder intersection was 514 (57%). Figure 10 contains a plot of the IHL POD and FAR scoring performance at each of the 23 NEXRAD sites for all PIREP reported positions located within 125 km from each site. Performance among the sites is fairly consistent and the average POD and FAR among all sites is 78% and 5%, respectively. Scoring results for the PIREPs located at radar ranges beyond 125 km (not shown) were similar to the results shown in Figure 10. This indicates that the Graupel with MII version of IHL performs effectively for this icing hazard scenario. In the absence of PIREPs, the algorithm is essentially a "virtual PIREP" for this icing hazard scenario available about every 4 to 10 minutes throughout the NEXRAD network within 125 km of each radar.

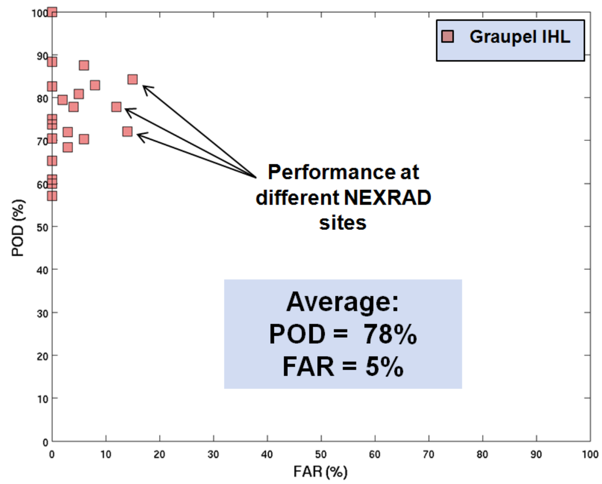

Figure 10. Scatter plot of the IHL algorithm performance for POD and FAR at each of the 23 NEXRAD sites studied for the subset of PIREPs located within 125 km range from each site and those reports where Graupel was detected within the cylinder footprint.

A categorical breakdown of all radar beam-cylinder comparisons located within 125 km range is shown in Figure 11 for the icing (left) and null (right) PIREPs, respectively. A significant portion of reports were not considered in the study because no radar beam angle intersected the cylinder space (15% for icing; 43% for null). The icing reports were cases in which the icing was either reported at low altitudes far out in range away from the radar and beneath the lowest elevation angle or at high altitudes close in range from the radar and above the highest beam angle (particularly when the radar operates in clear air mode scanning). The primary reason there was no beam angle intersection for nearly half of all null PIREPs is due to the significantly smaller cylinder size used in the comparisons to that used for icing PIREPs (see Figure 8). The smaller cylinder size was chosen to avoid extending the

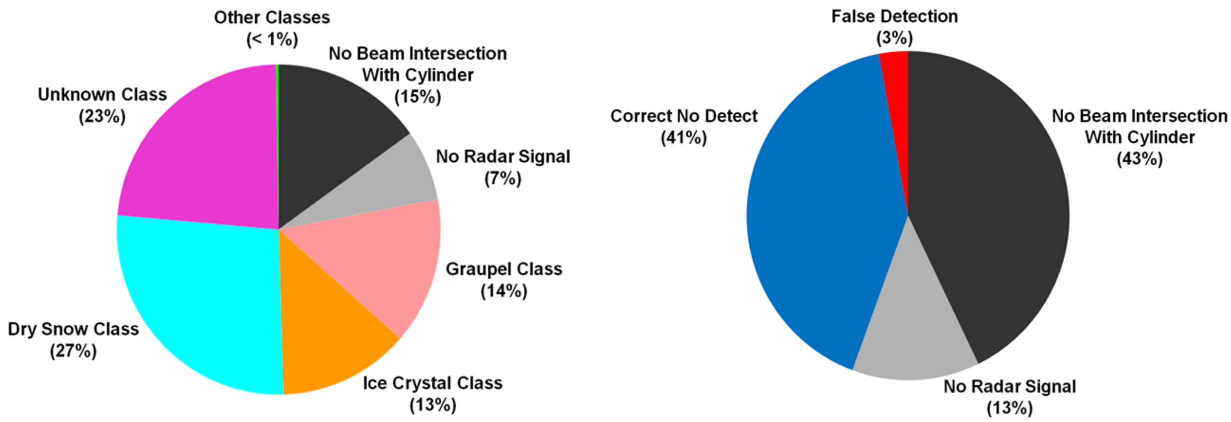

Figure 11. Pie charts showing the categorical breakdown of all radar-PIREP comparisons located within 125 km from the NEXRAD sites for icing (left) and null (right) PIREPs, respectively. The categorical frequency of reports when no elevation beam intersected the cylinder and when no radar signal was detected above the SNR (signal-to-noise ratio) within the cylinder was calculated for both report types. For all other comparisons, the frequencies of the majority HCA class associated with icing is shown on the left and the frequencies of the scoring measures for the no-icing observed reports is shown on the right.

reported no-icing area into nearby precipitation regions where icing may exist.

For the remainder of the reports, the radar dual pol smoothed reflectivity (SMZ) product and HCA classifications were analyzed among the bins that intersected the cylinder space. No valid SMZ values exceeding the signal-to-noise ratio (SNR) ('No Radar Signal' category) were found in 7% and 13% of the icing and null PIREPs, respectively. Among the icing reports where the radar bins contained valid SMZ values, the most frequent classification generated by the HCA was recorded to determine which classes were most often associated with the icing hazard. Figure 11 (left chart) shows that Graupel was the majority class in 14% of the PIREPs (and from which the POD described above was computed) but icing was most often reported in regions classified as Dry Snow (27%), Unknown (23%), and Ice Crystal (13%). Not surprisingly, these results clearly indicate that the IHL algorithm needs to incorporate additional methods to expand into the identification of the icing hazard for non-Graupel classified regions (i.e., the mixed phase icing hazard). For the remainder of null reports in which the radar bins contained valid SMZ values, Figure 11 (right chart) shows the fraction of reports for the IHL detection scoring categories, 'Correct No Detect' and 'False Alarm' was 41% and 3%, respectively.

3.3 Analysis of Reflectivity Observed and Icing PIREP Severity

Another objective of the IHL verification study was to analyze the SMZ product among the valid radar bins intersecting the cylinder space to determine how frequent the NEXRADs observed reflectivity in the aircraft icing reported regions. The same time (+/- 15 min) and space (Figure 8) tolerances used to assess the IHL algorithm performance were used here except the icing PIREP cylinder radius was reduced from 50 to 25 km to limit analysis to an area closer to the PIREP location. An important metric to determine is the ratio of valid SMZ radar bins containing a detectable echo (above the SNR) among all bins that intersect the cylinder. These results are shown in Figure 12. The blue histogram bars represent the distribution of all icing PIREPs located within 125 km from the NEXRAD sites separated by the severity of icing observed by the pilot. Severity level categories 1-3, 4-5, and 6-8 denote trace to light, light-moderate to moderate, and moderate-severe to severe icing, respectively. Light (level 3) and moderate (level 5) icing were the most frequent severity categories reported during the study interval. The red histogram bars show the corresponding frequency of PIREPs having detectable SMZ echo in at least 10% of the radar bins intersecting the cylinder. This does not mean HCA had Graupel classified when there were SMZ echoes. These results indicate a strong relationship between icing conditions and radar reflectivity detected by NEXRAD. However, as mentioned earlier, there is a limitation on the usefulness of PIREP-radar comparisons given the inherent space-time resolution uncertainty of aircraft reported icing.

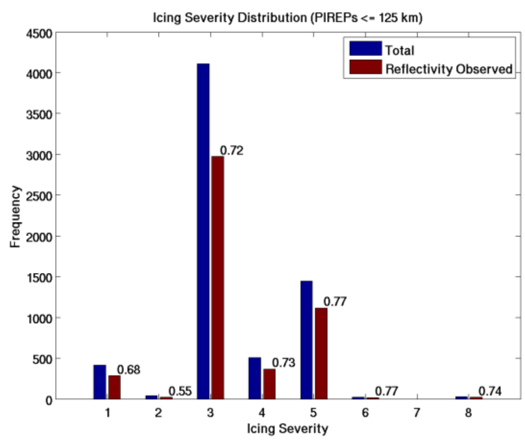

Figure 12. Number of PIREPs located within 125 km from a NEXRAD site grouped by icing severity index determined by the pilot (blue bars) and fraction of total reports for which SMZ echoes were detected in at least 10% of all radar bins intersecting the cylinder (red bars).

The fraction of PIREPs containing at least 10% detectable reflectivity were differentiated further according to the radar VCP operational scanning mode and by the mean SMZ value binned into 5 dBZ intervals. These results are shown in the frequency distribution histograms in Figure 13 for precipitation mode scanning (left) and clear air mode scanning (right). The distributions are separated by icing severity level, increasing from trace icing (level 1) at the bottom to severe icing (level 8) at the top. The far left column in each distribution (labeled NE) contains the number of reports with no detectable SMZ echo within the cylinder space. Independent of the VCP mode, the most frequent mean SMZ values were between 0-10 dBZ. The distributions also show that the increased sensitivity of clear air mode scanning enables the radar to detect icing hazards associated with lower reflectivity that would otherwise not be possible in precipitation mode scanning. Further study is needed to explore the parameters that indicate when the improved sensitivity of clear air scanning by NEXRAD should become the default for winter weather monitoring.

4. COMPARISON OF HCA CLASSIFICATIONS TO IN SITU OBSERVED ICING

MIT LL partnered with the National Research Council of Canada (NRC) in February 2013 to conduct three first-ever radar-directed in situ icing missions within range of the dual pol Buffalo, New York NEXRAD (KBUF). Figure 14 illustrates a plan view of the flight tracks during each mission date originating and ending in Ottawa, Canada. The purpose of the campaign was to direct the NRC Convair 580 aircraft into distinct winter weather systems for the purpose of quantifying the microphysical properties for verification of the presence of SLW and for interpretation of the correct hydrometeor classification. Williams et al. (2015) contains an in-depth summary of this field campaign. For the purposes of this study, three comparative examples of KBUF hydrometeor classifications and aircraft measurements of liquid water content (LWC) from the onboard Nevzorov probe (Korolev et al. 1998), one from each mission, are presented. The results illustrate similar findings to that obtained in the PIREP-radar comparisons in the previous section, namely that the HCA Graupel class alone does not fully expose the icing hazard. In other words, HCA is not yet developed to accommodate a portion of the mixed phase spectrum of scenarios.

The first flight mission took place in the morning hours on February 19, 2013 with the strategy to fly the Convair in fixed altitude trajectories to sample the horizontal variations of SLW. The targeted zone was north and west of KBUF within a wide, eastward moving snow band

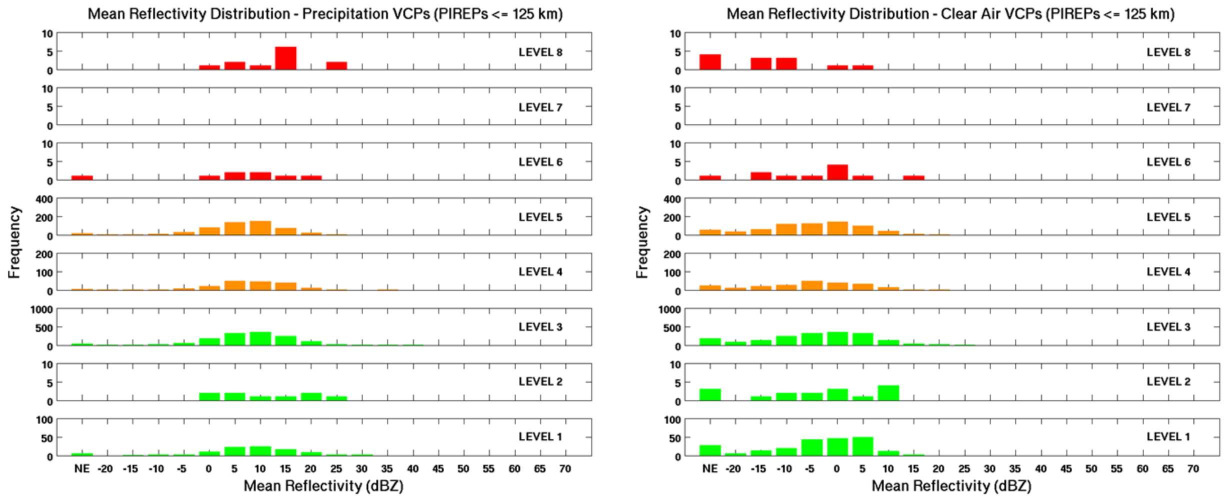

Figure 13. Frequency distributions showing the number of PIREPs associated with detectable SMZ (smoothed reflectivity) echoes in at least 10% of the radar bins intersecting the cylinder for all reports within 125 km from a NEXRAD site while the radar was scanning in precipitation mode (left) and clear air mode (right). SMZ values are binned into 5 dBZ intervals and the number of reports where no detectable reflectivity was found is shown in the far left column (NE). Distributions are separated by icing severity level from trace (green) at the bottom to severe (red) at the top.

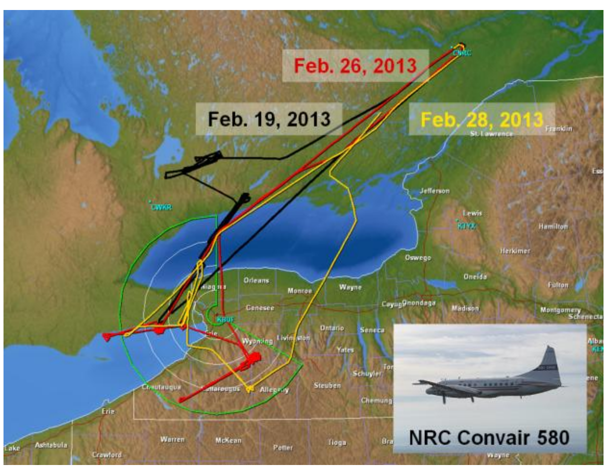

Figure 14. An overview of the three aircraft icing mission flight tracks conducted by the NRC Convair 580 near the Buffalo, New York NEXRAD.

area propagating ahead of a cold front. The regions sampled were predominately classified by HCA as Dry Snow. The top plot in Figure 15 contains five-second observations of the aircraft measured LWC (red line), temperature (blue line), and the majority class detected by the KBUF HCA (thick line color-coded by class) within a small 15 range bin spatial window centered at the Convair position for the period 14:10-14:20 UTC. The HCA class abbreviations are defined as: Biological (BI), Ground Clutter (GC), Ice Crystal (IC), Dry Snow (DS), Wet Snow (WS), Rain (RA), Heavy Rain (HR), Big Drops (BD), Graupel (GR), Hail-Rain mix (HA), and Unknown (UK). The three-panel PPI plots show the KBUF HCA product centered on the Convair flight segment (black line) and coinciding with the start (14:10; left), middle (14:15; center) and end (14:20; right) periods within the above aircraft measurement line plots. The imagery strips beneath each HCA PPI plot are time coincident black and white projections of the hydrometeor particles collected by the aircraft Optical Array Probes (OAP). During this ten-minute interval, the aircraft altitude is nearly fixed at 1425 m and the temperature is stable at -2° C. The LWC is negligible at 14:10 UTC but steadily increases to a maximum of 0.44 g/m^3 at 14:19 UTC. The majority class detected by HCA is predominately Dry Snow (shown as turquoise) along the flight segments with intermittent Ice Crystal (orange) and Unknown (magenta) classified regions toward the end of the interval. This episode of pronounced LWC along the flight track indicates that the HCA Dry Snow class is masking the existence of a mixed phase condition and the underlying icing hazard.

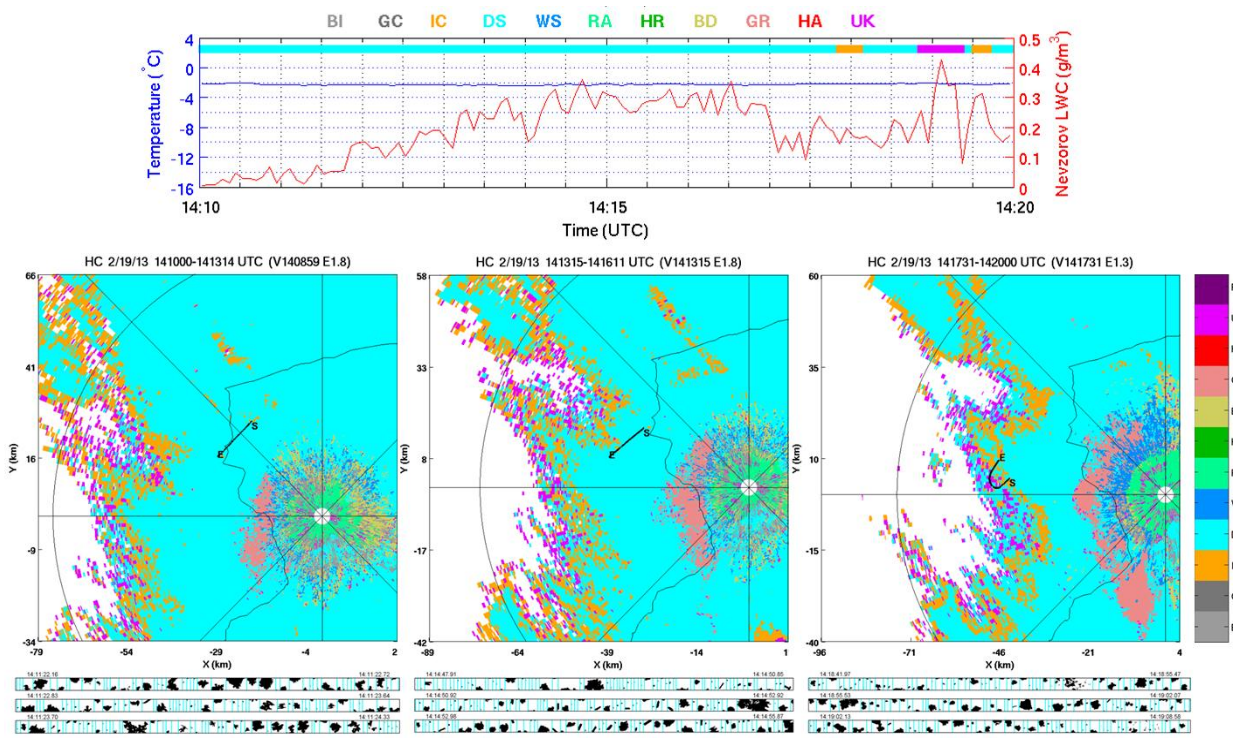

Figure 15. Comparison of aircraft in situ measurements and HCA classifications for the first flight mission on February 19, 2013 for the period 14:10-14:20 UTC. The top plot shows five-second observations of LWC (red line), temperature (blue line), and the majority HCA class detection spatially matched to the Convair position (thick color-coded horizontal line). The three-panel PPI plots show the HCA product coinciding with the start, middle, and end periods within the line plot interval shown at the top. The black solid line in each plot shows the Convair flight track position mapped nearest in altitude to the radar elevation PPI shown. The image strips beneath each PPI plot show the time coincident projection of hydrometeor particles collected by the Optical Array Probe sensor.

During the second flight, the KBUF region was dominated by a large swath of mixed phase precipitation advancing north ahead of a large low pressure system situated in the lower Mid-West states. The flight mission objective was to perform multiple spiral maneuvers into and out of the ML zone in regions largely classified as Graupel. Following the same plot structure described for Figure 15, Figure 16 contains a ten-minute interval of aircraft measurements and HCA class detections for the first flight segment descent into the ML between 00:40-00:50 UTC on February 27, 2013. The temperature is near -5° C at the start of the interval and slowly increases during descent toward 0° C by 00:46 UTC. The HCA is identifying these regions as Dry Snow. Once the aircraft nears the ML, the majority class is identified as Graupel (pink). Throughout much of the interval, the measured LWC is weak, but not negligible, averaging near 0.05 g/m^3. The OAP imagery shows a transition of irregular shaped ice crystal aggregates in the Dry Snow classified region to mixed ice crystal aggregates and small spherical particles in the Graupel classified region. Similar to the February 19th flight, the LWC and OAP observations both confirm that mixed phase conditions occurred throughout the interval. Compared to February 19, this encounter is with less SLW yet conditions were such to lead to graupel formation and HCA classification of Graupel. There was air traffic control dialogue with commercial flights in the area about potential icing hazards.

In situ sampling of the third storm event occurred on February 28, 2013 when the Buffalo area received lighter precipitation from the slow moving remnants of the previous day's system

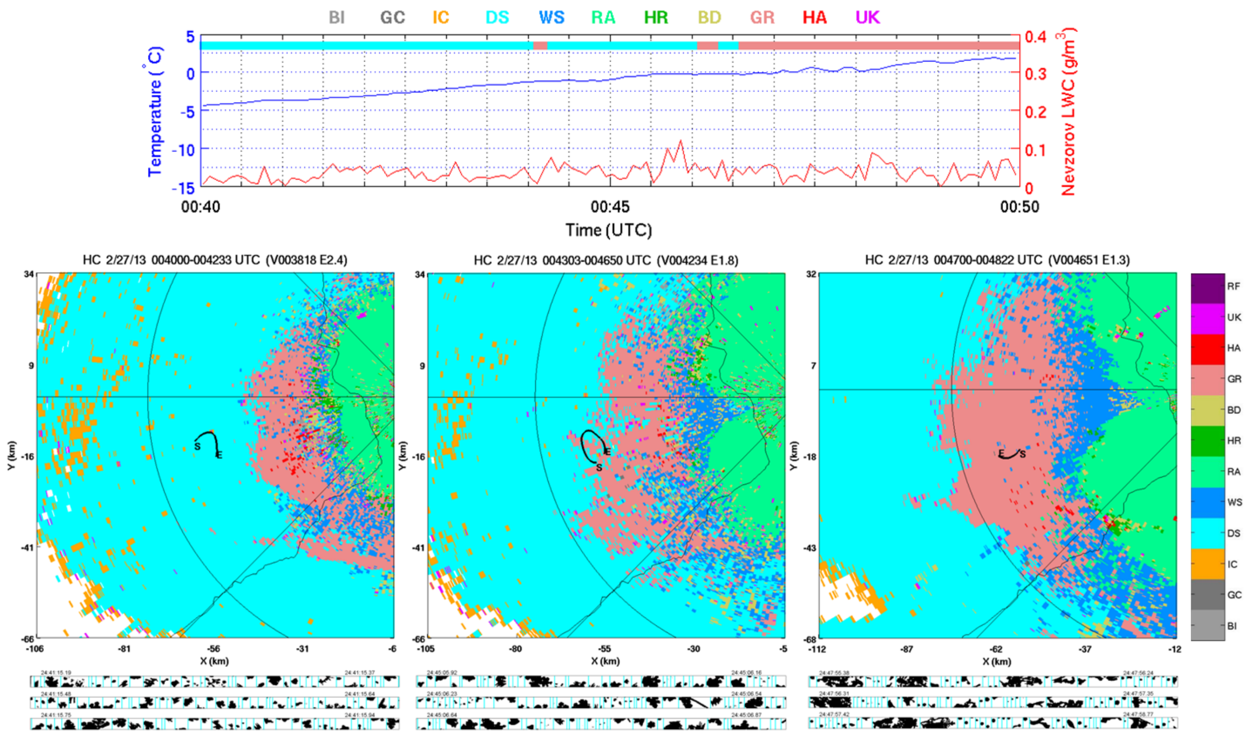

Figure 16. Comparison of aircraft in situ measurements and HCA classifications for the second flight mission on February 27, 2013 for the period 00:40-00:50 UTC. See Figure 15 caption for a description of the figure layout.

described above. The flight mission performed 'porpoising' (lateral up and down sequence) maneuver flight tracks to expose the layered structure of SLW and quasi-uniform ice crystal populations. Figure 17 depicts the aircraft measurements and HCA detections for the ten-minute interval 19:20-19:30 UTC. The temperature oscillation reveals the change in aircraft altitude over the period and the Nevzorov probe recorded multiple episodes of significant (>0.1 g/m^3) LWC with a maximum of 0.53 g/m^3 at 19:28 UTC. As evidenced by the OAP imagery strips and HCA PPI plots, the Convair flew through populations of dendrite and needle ice crystals in regions classified alternately as Unknown, Dry Snow, and Ice Crystal. The observations of dendrites and needles follows intersection with temperatures associated with those crystal types expected as described by crystal habit diagrams. The undulation pattern of negligible to peak values in LWC do not coincide with HCA transitions from one hydrometeor class to the next but rather occur within longer segments of a single classification with maximum readings occurring in longer Dry Snow and Ice Crystal episodes. This behavior was repeated throughout the flight.

The in situ missions clearly identified the HCA classifications that are candidates of focus regarding mixed phase identification. Toward understanding the frequency with which a particular HCA class will include SLW, all temporal and spatially matched five-second aircraft measurements of LWC and HCA radar classifications collected over the three missions were compared for four broadly sampled categories (above the ML), Ice Crystal, Dry Snow, Graupel, and Unknown. Relative frequency distributions of LWC for each HCA category are shown in Figure 18 and grouped into four measurement intervals defined as None (<0.005 g/m^3), Very Weak (0.005-0.05 g/m^3), Weak (0.05-0.1 g/m^3), and Significant (≥0.1 g/m^3).

The Ice Crystal distribution shows a majority of observations (62%) contained no LWC and the

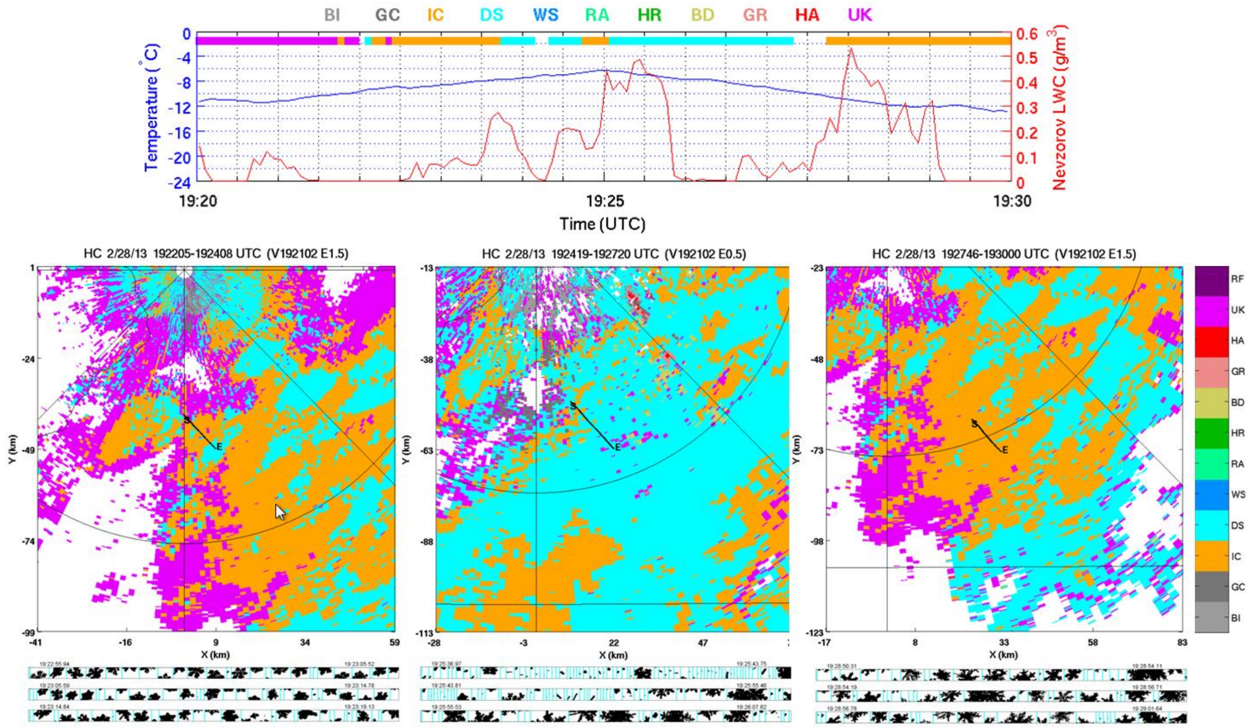

Figure 17. Comparison of aircraft in situ measurements and HCA classifications for the third flight mission on February 28, 2013 for the period 19:20-19:30 UTC. See Figure 15 caption for a description of the figure layout.

least likely HCA category among the four to be associated with significant icing. Dry Snow was the most frequently sampled classification region with a near equal division of encounters having no LWC (44%) and some relevant level of LWC observed. Although Graupel was the least sampled region, the LWC distribution notably shows a high percentage of encounters (93%) had measurable LWC lending confidence on its use within the IHL algorithm. Lastly, the LWC distribution for the Unknown class, the default category when the discrimination between hydrometeor types is not possible, shows similar results to the Dry Snow class in that a significant number of observations contained both negligible and significant icing with the encounters. These important results suggest further examination of the dual pol products and an improved fidelity in HCA classification is necessary to extract a mixed phase subclass within the existing HCA categories.

5. SUMMARY

The baseline IHL algorithm operates within the NEXRAD ORPG system and creates a high resolution temporal and spatial icing detection product that identifies the top and bottom altitudes of an icing layer determined by the radar beam altitudes where Graupel was classified by the NEXRAD HCA. The top altitude can be extended vertically if favorable MII conditions, derived from temperature and relative humidity NWP model information, exist above the region where Graupel was detected. MII essentially is a proxy approach for including some mixed phase region above detectable Graupel. The IHL product is generated once per radar volume (every 4 to 10 minutes) and is not meant to be a stand-alone product but rather serve as additional information to external systems that provide aviation hazard information for the FAA.

The focus of this study was to assess the performance of the IHL algorithm using aircraft

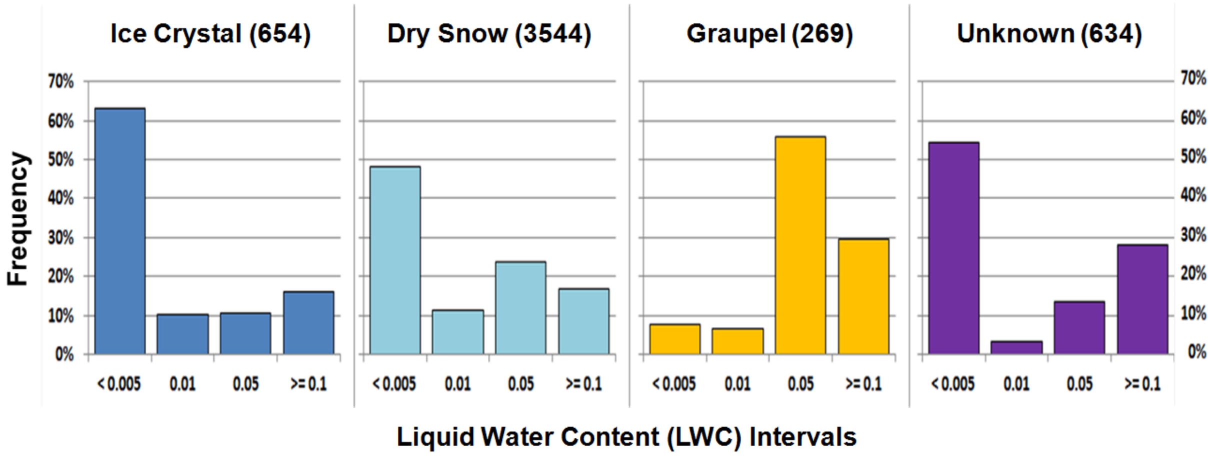

Figure 18. Relative frequency distributions of five-second aircraft measurements of LWC and HCA classification comparisons collected over the three flight missions. Distributions are shown for the hydrometeor classes, Ice Crystal, Dry Snow, Graupel, and Unknown. The number of comparisons is provided next to each class title.

icing PIREPs for verification. Reports collected over a two-month period in close proximity to 23 NEXRAD sites located in high icing incident reported regions were analyzed. A methodology was adopted to capture the spatial and temporal uncertainties of PIREPs with an icing cylindrical area from which the IHL icing altitude detections can be compared and evaluated. For the subset of reports overlapping with HCA Graupel classifications (14%), the average POD and FAR among all NEXRAD sites studied was 78% and 5%, respectively. For all other PIREPs in which there were sufficient radar returns exceeding the SNR within the cylindrical area and not classified as Graupel, the predominate HCA class and corresponding frequency associated with the icing hazard were Dry Snow (27%), Unknown (23%), and Ice Crystal (13%).

Comparisons between the mean of the dual pol smoothed reflectivity and reported icing severity differentiated by the radar VCP operating mode revealed icing hazards associated with low reflectivity winter storm events may be better observed with clear air scanning rather than with precipitation mode scanning. VCP issues such as the cone-of-silence and overshooting more shallow winter weather at far range cannot be overcome in NEXRAD. However, the NEXRAD community has designed a new winter-intended clear air VCP that will complete in 20% less time (8 minutes), retain the sensitivity advantage, and scan to higher elevations to somewhat mitigate the severe cone-of-silence in the current clear air VCPs. The new VCP could debut in 2017.

Comparisons between aircraft in situ measurements of LWC and KBUF HCA classifications showed various levels of icing encountered among the non-Graupel classes, specifically Dry Snow and Unknown. These results, in conjunction with the non-Graupel class distributions associated with icing in the PIREP study, suggest additional methods to identify mixed phase conditions within the dual pol products are necessary to improve fidelity in HCA classification and subsequently enhance icing hazard detection in the IHL algorithm.

6. REFERENCES

Bernstein, B. C., F. McDonough, M. K. Politovich, B. G. Brown, T. P. Ratvasky, D. R. Miller, C. A. Wolff, and G. Cunning, 2005: Current Icing Potential: Algorithm Description and Comparison with Aircraft Observations. *J. Appl. Meteor.*, **44,** 969–986.

Brown, B. G., G. Thompson, R. T. Bruintjes, R. Bullock, and T. Kane, 1997: Intercomparison of

In-Flight Icing Algorithms. Part II: Statistical Verification Results, *Wea. Forecasting*, **12**, 890-914.

Ganger, T., M. J. Istok, S. Shema, and B. Bumgarner, 2002: The WSR-88D Common Operations and Development Environment - Status and Future Plans, 18th Conf. On Interactive Information Processing Systems, January 2002, Orlando, FL.

Giangrade, S. E., J. M. Krause, and A. V. Ryzhkov, 2008: Automatic Designation of the Melting Layer with a Polarimetric Prototype of the WSR-88D Radar. *J. Appl. Meteor.*, **47**, 1354-1364.

Hallowell, R. G., M. F. Donovan, D. J. Smalley, and B. J. Bennett, 2013: Icing Hazard Detection with NEXRAD IHL. *Proc. American Meteorological Society's 36th International Radar Conference, Breckenridge, CO.*

Korolev, A.V., J.W. Strapp, G.A. Issac, and A.N. Nevzorov, 1998: The Nevzorov Airborne Hot Wire LWC-TWC Probe: Principles of Operation and Performance Characteristics. J. Atmos. Ocean. Tech., 15, 1495-1510.

Park, H., A.V. Ryzhkov, D.S. Zrnic, and K-E. Kim, 2009: The Hydrometeor Classification Algorithm for the Polarimetric WSR-88D: Description and Application to an MCS. *Wea. Forecasting*, **24**, 730–748.

Schwartz, B, 1996: The Quantitative Use of PIREPs in Developing Aviation Weather Guidance Products, *Wea. Forecasting*, **11**, 372-384.

Smalley, D. J. and B. J. Bennett, 2002: Using ORPG to Enhance NEXRAD Products to Support FAA Critical Systems. *Proc. American Meteorological Society's 10th Conference on Aviation, Range, and Aerospace Meteorology, Portland, OR.*

Williams, E. R., M. F. Donovan, D. J. Smalley, R. G. Hallowell, E. P. Griffin, K. T. Hood, B. J. Bennett, 2015: The 2013 Buffalo Area Icing and Radar Study (BAIRS). MIT Lincoln Laboratory Project Report ATC-419, 132 pp.